Mechanical properties and reliability of glass-ceramic foam scaffolds for bone repair

Mechanical properties and reliability of glass-ceramic foam scaffolds for bone repair

Francesco Baino, Chiara Vitale-Brovarone*

Institute of Materials Physics and Engineering, Applied Science and Technology Department, Politecnico di Torino, Corso Duca degli Abruzzi 24, 10129 Torino, Italy

*Corresponding author: C. Vitale-Brovarone

Tel.: +39 011 564 4716

Fax: +39 011 564 4624

E-mail: chiara.vitale@polito.it

Abstract

The development of reliable, synthetic scaffolds to repair large defects in load-bearing bones is one of the key challenges of regenerative medicine of hard tissues. This study addresses the mechanical properties of experimental glass-ceramic scaffolds fabricated by sponge replication and exhibiting a bone-like 3-D trabecular architecture, as assessed by micro-computed tomography investigations. The scaffolds have a strength of 18 MPa, an elastic modulus around 380 MPa, a Weibull modulus of 4 and a fracture energy of 544 kJ m^{-3} when tested in compression. Such results were compared with and found similar or even superior to those reported in the literature for bioceramic scaffolds and human cancellous bone. These key mechanical data, together with the peculiar foam-like porous architecture, indicate the great potential of this type of scaffolds for use in load-bearing bone tissue engineering applications.

Keywords: Glass; Scaffold; Compressive strength; Weibull modulus; Bone tissue engineering

1. Introduction

Since Hench and associates first described, in the early 1970s, the ability of 45S5 Bioglass® to form an interfacial bond with host tissues *in vivo* [1], bioactive glasses (BGs) with various oxide formulations have attracted increasing interest among biomaterials researchers [2]. Upon implantation, silicate BGs undergo specific reactions leading to the formation of an amorphous calcium phosphate or hydroxyapatite (HA) layer on the surface of the glass, which is responsible for

their strong bonding with the surrounding tissues [1]. BGs are particularly interesting for bone tissue engineering applications as they have been recognized able to promote the proliferation and differentiation of bone cells [3], to release ions activating osteogenic genes expression [4] and to stimulate angiogenesis [5].

From a general viewpoint, the physico-chemical and mechanical properties of BGs can be tailored over a wide range by changing either composition or thermal/environmental processing history. In 2006, Park et al. [6] and Chen et al. [7] independently pioneered the fabrication of BG-derived macroporous scaffolds by polymeric sponge replication; since then, several other manufacturing methods [8], including the use of pore-former polymeric particles [9,10], freeze-drying [11] and lithography-based approaches [12], have been proposed. The architectural design of a scaffold is a great challenge because, from a structural viewpoint, two competing requirements are to be fulfilled: on one hand, the scaffold should exhibit an adequate mechanical competence, e.g. strength and stiffness comparable to those of natural bone, but, on the other hand, the implant should be sufficiently porous to allow cells colonization and new bone in-growth once implanted in the human body. Apart from a few excellent exceptions [13], in the literature there is a relative paucity of publications reporting a comprehensive assessment of the mechanical properties of bioceramic scaffolds, as most studies have focused on evaluating only the compressive strength.

In the present work, foam-like glass-ceramic scaffolds based on an experimental silicate glass were fabricated by sponge replication and mechanically characterized assessing not only their compressive strength but also, for the first time, their elastic modulus, fracture energy and Weibull modulus, which are all key features to be taken into account for a rational design of porous brittle biomaterials.

2. Materials and methods

The material used for scaffold preparation is a silicate quaternary glass having the following molar composition: $57SiO_2$-$34CaO$-$6Na_2O$-$3Al_2O_3$. The glass reagents (high-purity powders of SiO_2, $CaCO_3$, Na_2CO_3, Al_2O_3 purchased from Sigma-Aldrich) were molten in a platinum crucible at 1550 °C for 1 h in air; the melt was quenched in cold water to obtain a frit, that was subsequently ground by a 6-balls zirconia milling machine and sieved to a final particle size below 32 μm.

Sponge replication method was adopted to fabricate the scaffolds according to a processing schedule reported elsewhere [14]. Briefly, 10-mm cubic blocks of a commercial open-cells polyurethane (PU) sponge (foam density ~20 kg m^{-3}) were soaked into a water-based glass slurry (weight composition: 30% glass, 64% distilled water, 6% poly(vinyl alcohol)) and subsequently compressed to squeeze the slurry out of the pores in a controlled way. After drying at room

temperature in air, the samples were thermally treated (1000 °C/3 h, heating rate 5 °C min^{-1}) to remove the polymeric sponge and to sinter the glass particles, thereby obtaining a glass-ceramic replica of the template.

Samples shrinkage due to sintering was assessed by geometrical measurements as $(1-V_s/V_0)\times 100$, wherein V_0 is the volume of the glass-impregnated sponge before sintering and V_s is the volume of the sintered scaffold.

The scaffolds were chromium-coated, and their morphology and porous 3-D architecture were investigated by scanning electron microscopy (SEM, Philips 525 M; accelerating voltage = 15 kV). The inner porous network of the scaffolds was also non-destructively investigated by micro-computed tomography (micro-CT; SkyScan 1174, Micro Photonics Inc.) to assess the pores content.

The compressive failure stress σ_c (MPa) was evaluated through crushing tests on 7 mm × 7 mm × 7 mm cubic samples (MTS System Corp. apparatus, 5-kN cell load, cross-head speed set at 1 mm min^{-1}) as:

$$\sigma_c = \frac{L_M}{A_R} \tag{1}$$

being L_M (N) the maximum load registered during the test and A_R (mm^2) the resistant cross-sectional area. Prior to testing the contact surfaces of the scaffolds were polished using SiC grit papers to obtain parallel surfaces.

The elastic modulus was determined from the linear region of the stress-strain response. This approach is commonly used and accepted in the literature [13,15] although leading to underestimation of the elastic modulus; some authors suggested alternative strategies, such as ultrasonic characterization, to partially solve this problem [16].

The energy per unit volume E_V (J mm^{-3}) absorbed by the scaffold till the breaking off is reached was defined as the energy necessary to deform a specimen from the unloaded condition to the failure strain ε_f, and was calculated as the area under the stress-strain curve up to ε_f [17]:

$$E_V = \int_0^{\varepsilon_f} \sigma(\varepsilon) d\varepsilon \tag{2}$$

being the strain ε the integration variable; the initial and final condition are, respectively, $\sigma(\varepsilon = 0) = 0$ and $\sigma(\varepsilon = \varepsilon_f) = \sigma_c$ (calculated from Eq.(1)).

The above-mentioned mechanical parameters were expressed as mean value ± standard deviation calculated on thirty samples.

The Weibull modulus was determined according to ASTM C1239-07 [18] by fitting the strength data with the equation:

$$\ln\ln\left(\frac{1}{1-P_f}\right) = m\ln\left(\frac{\sigma}{\sigma_0}\right) = m\ln(\sigma) - m\ln(\sigma_0) \tag{3}$$

wherein P_f is the probability of failure at a stress σ and σ_0 is the Weibull scale parameter determined from the intercept of the fit to the data and the Weibull modulus *m*. The probability of failure was evaluated using the equation $P_f = \frac{j - 0.5}{n}$, wherein *n* is the total number of tested specimens and *j* is the specimen rank in ascending order of failure stresses.

3. Results and discussion

The scaffold volumetric shrinkage was estimated to be 67 ± 5 %, the low standard deviation demonstrated the good reproducibility of the adopted fabrication method.

Fig. 1a reports a SEM micrograph of scaffold surface, exhibiting a trabecular-like porous architecture mimicking that of cancellous bone. A homogeneous, bimodal distribution of pores sizes – pores above 100 μm originated by the 3-D macro-cells network of the PU template and pores below 10-20 μm – is clearly evident in the scaffold cross-section (Fig. 1b). Fig. 1c puts into evidence the typical needle-like shape of 10-μm long wollastonite ($CaSiO_3$) crystals developed during thermal treatment [14], which demonstrates the glass-ceramic nature of the scaffold material.

Micro-CT analysis (Figs. 1d,e) revealed a mean macro-pore size of 240 μm (the majority of small micro-pores visible in Fig. 1b were excluded from the calculation adopting an image resolution of 10 μm) and a total porosity of 56 ± 6 vol.%, which is comparable to that of healthy trabecular human bone (50-80 vol.% [19]). Scaffolds had a good 3-D pores interconnectivity throughout the whole volume (Fig. 1e) with open porosity above 95 % of the overall pores content, which is a key feature after *in vivo* implantation in order to have paths for cells to migrate, tissue to grow in and waste products to flow out.

A typical example of compressive stress-strain curve for SCNA scaffold is reported in Fig. 2. The curve exhibits a multi-peak profile, which is peculiar of foam-like ceramics [20]. The curves have a positive slope up to a first peak, after which the thin trabeculae begin to crack causing an apparent stress drop (negative slope); however, the scaffold was still able to withstand higher loads and therefore the stress rises again. The repetition of this behaviour produces a jagged stress-strain curve while the progressive cracking of scaffold struts occurs; when also the thick trabeculae are fractured, the curve has an ultimate negative slope.

The scaffolds compressive strength was 18 ± 5 MPa, which is above the standard reference range (2-12 MPa [21]) considered for human trabecular bone as well as most foam-like scaffolds with the same porosity reported in the literature [8,22]. The elastic modulus, 380 ± 172 MPa, is within the range assessed for cancellous bone (50-500 MPa [23]); this is an important finding as one of the major reasons leading to implant failure is the stiffness mismatch

between implanted biomaterial and surrounding bone. The fracture energy was 544 ± 230 kJ m^{-3}, which is 4 to 25 times higher than that reported for glass-ceramic scaffolds having analogous porous architecture [24,25].

Fig. 3 shows Weibull plot of the compressive strength data; least mean squares fitting of a straight line through the experimental points gave a Weibull modulus of 4. The Weibull modulus determined from the strength data for a large number of identical samples (typically 20-30 or more) is commonly used as a measure of the mechanical reliability or the probability of failure of brittle materials [26]. The mechanical response of brittle materials is sensitive to microstructural flaws such as pores and micro-cracks: therefore, Weibull modulus is used to evaluate the probability of failure of brittle materials under a given stress. In this work, the Weibull modulus of glass-ceramic scaffolds produced by sponge replication was assessed for the first time, hence a direct comparison with analogous data from the literature is not possible; nonetheless, a few results concerning bioceramic scaffolds produced by different techniques can be considered. The Weibull moduli of solid-freeform-fabricated (SFF) porous HA, β-TCP and calcium polyphosphates scaffolds have been reported to be within 3-9 for testing in compression [27-29]. To the best of the authors' knowledge, only one study reporting the Weibull modulus of bioactive glass scaffolds is available in the literature: specifically, Liu et al. [13] recently assessed a Weibull modulus around 12 for robocast 13-93 glass scaffolds. This value is significantly higher compared to that assessed for SCNA scaffolds; however, it has to be taken into account that the porosity of 13-93 glass scaffolds is quite lower (47 vol.% [13]) and, most importantly, the methods of fabrication and subsequent 3-D porous architectures and struts microstructures are far different: robocast scaffolds are constituted by dense glass filaments that are free from large flaws, whereas a diffused micro-porosity can be observed along the cross-section of SCNA scaffolds struts (Fig. 2). The increase of sintering temperature and time might allow to reduce the small micro-pores of SCNA scaffolds thereby contributing to further improve the mechanical properties; however, a higher shrinkage involving a lower porosity would be also achieved, which would make the scaffolds unsuitable for bone tissue engineering applications.

Looking at the future, a significant increment of Weibull modulus could be achieved by polymer infiltration of sintered SCNA foams, as suggested by Martinez-Vazquez et al. [28] who investigated the effect of poly(lactic acid) and poly(ε-caprolactone) coatings on β-TCP foams. On the other hand, the scaffold toughness will increase *in vivo*: Woodard et al. [30] reported that porous bioceramic scaffolds, with a brittle response as fabricated, show an elastoplastic response in compression after implantation for 2 months in pigs.

The results reported in this paper further support the mechanical suitability of SCNA scaffolds as load-bearing high-strength grafts for bone defect filling and, moreover, as trabecular-like coatings on prosthetic devices for better osteointegration, as recently proposed by the authors [31,32].

4. Conclusions

SCNA scaffolds fabricated by sponge replication exhibited a foam-like 3-D porous network mimicking the trabecular architecture of cancellous bone. The total porosity, which was predominantly open, was around 56 vol.% and the pore sizes ranged within 100-500 μm. When tested under compression, the scaffolds had a strength of 18 MPa, an elastic modulus around 380 MPa, a Weibull modulus of 4 and a fracture energy of 544 kJ m^{-3} (mean values). Besides providing key data for the design of bioactive glass porous grafts, these findings support the mechanical suitability of the produced scaffolds for load-bearing bone repair.

Acknowledgements

This work was supported by the EU-funded project MATCh ("Monoblock acetabular cup with trabecular-like coating", Grant no. 286548).

References

[1] Hench LL. The story of Bioglass®. J Mater Sci: Mater Med 2006;17:967-78.

[2] Jones JR. Review of bioactive glass: from Hench to hybrids. Acta Biomater 2013;9:4457-86.

[3] Rahaman MN, Day DE, Bal BS, Fu Q, Jung SB, Bonewald LF and Tomsia AP. Bioactive glass in tissue engineering, Acta Biomater 2011;7:2355-73.

[4] Hoppe A, Güldal NG and Boccaccini AR. A review of the biological response to ionic dissolution products from bioactive glasses and glass-ceramics. Biomaterials 2011;32:2757-74.

[5] Gorustovich A, Roether J, Boccaccini AR. Effect of bioactive glasses on angiogenesis: in-vitro and in-vivo evidence - a review. Tissue Eng B 2010;16:199-207.

[6] Park YS, Kim KN, Kim KM, Choi SH, Kim CK, Legeros RZ, Lee YK. Feasibility of three dimensional macroporous scaffold using calcium phosphate glass and polyurethane sponge. J Mater Sci: Mater Med 2006;41:4357-64.

[7] Chen Q, Thompson ID, Boccaccini AR. 45S5 Bioglass®-derived glass-ceramic scaffolds for bone tissue engineering. Biomaterials 2006;27:2414-25.

[8] Baino F and Vitale-Brovarone C. Three-dimensional glass-derived scaffolds for bone tissue engineering: current trends and forecasts for the future. J Biomed Mater Res A 2011; 97: 514-535.

[9] Baino F, Verné E and Vitale-Brovarone C. 3-D high strength glass-ceramic scaffolds containing fluoroapatite for load-bearing bone portions replacement. Mater Sci Eng C 2009;29:2055-62.

[10] Bellucci D, Cannillo V, Sola A, Chiellini F, Gazzarri M and Migone C. Macroporous Bioglass®-derived scaffolds for bone tissue regeneration. Ceram Int 2011;37:1575-85.

[11] Liu X, Rahaman MN, Fu Q, Tomsia AP. Porous and strong bioactive glass (13-93) scaffolds prepared by unidirectional freezing of camphene-based suspensions. Acta Biomater 2012;8:415-23.

[12] Tesavibul P, Felzmann R, Gruber S, Liska R, Thompson I, Boccaccini AR et al. Processing of 45S5 Bioglass® by lithography-based additive manufacturing. Mater Lett 2012;74:81-4.

[13] Liu X, Rahaman MN, Hilmas GE, Bal BS. Mechanical properties of bioactive glass (13-93) scaffolds fabricated by robotic deposition for structural bone repair. Acta Biomater 2013;9:7025-34.

[14] Ma H, Baino F, Fiorilli S, Vitale-Brovarone C, Onida B. Al-MCM-41 inside a glass-ceramic scaffold: a meso-macroporous system for acid catalysis. J Eur Ceram Soc 2013;33:1535-43

[15] Doblare M, Garcia JM, Gomez MJ. Modelling bone tissue fracture and healing: a review. Eng Fract Mech 2004;71:1809-40.

[16] Kohlhauser C, Hellmich C, Vitale-Brovarone C, Boccaccini AR, Rota A, Eberhardsteiner J. Ultrasonic characterisation of porous biomaterials across different frequencies. Strain 2009;45:34-44.

[17] Kenesei P, Kadar C, Rajkovits Z and Lendvai J. The influence of cell-size distribution on the plastic deformation in metal foams. Scripta Mater 2004;50:295-300.

[18] ASTM C1239-07. Standard practice for reporting uniaxial strength data and estimating Weibull distribution parameters for advanced ceramics.

[19] Karageorgiou V, Kaplan D. Porosity of 3D biomaterial scaffolds and osteogenesis. Biomaterials 2005;26:5474-91.

[20] Rice R. Mechanical properties. In: Schaufer, Colombo P, editors. Cellular ceramics: structure, manufacturing, properties and applications, New York: Wiley; 2005, p. 291-312.

[21] Hench LL, Wilson J. An introduction to bioceramics. Singapore: World Scientific; 1993.

[22] Baino F, Ferraris M, Bretcanu O, Verné E, Vitale-Brovarone C. Optimization of composition, structure and mechanical strength of bioactive 3-D glass-ceramic scaffolds for bone substitution. J Biomater Appl 2013;27:872-90.

[23] Thompson ID, Hench LL. Mechanical properties of bioactive glasses, glass-ceramics and composites. Proc Inst Mech Eng H 1998;212:127-37.

[24] Vitale-Brovarone C, Ciapetti G, Leonardi E, Baldini N, Bretcanu O, Verné E and Baino F. Resorbable glass-ceramic phosphate-based scaffolds for bone tissue engineering: synthesis, properties and in vitro effects on human marrow stromal cells. J Biomater Appl 2011; 26: 465-489.

[25] Bretcanu O, Baino F, Verné E, Vitale-Brovarone C. Novel resorbable glass-ceramic scaffolds for hard tissue engineering: from the parent phosphate glass to its bone-like macroporous derivatives. J Biomater Appl, in press. DOI: 10.1177/0885328213506759

[26] Wachtman JB, Cannon WR, Matthewson MJ. Mechanical properties of ceramics. 2nd ed. New York: Wiley; 2009.

[27] Miranda P, Pajares A, Saiz E, Tomsia AP, Guiberteau F. Mechanical properties of calcium phosphate scaffolds fabricated by robocasting. J Biomed Mater Res A 2008;85:218-27.

[28] Martinez-Vazquez FJ, Perera FH, Miranda P, Pajares A, Guiberteau F. Improving the compressive strength of bioceramic robocast scaffolds by polymer infiltration. Acta Biomater 2010;6:4361-8.

[29] Shanjani Y, Hu Y, Pilliar RM, Toyserkani E. Mechanical characteristics of solid-freeform-fabricated porous calcium polyphosphate structures with oriented stacked layers. Acta Biomater 2011;7:1788-96.

[30] Woodard JR, Hilldore AJ, Lan SK, Park CJ, Morgan AW, Eurell JA, et al. The mechanical properties and osteoconductivity of hydroxyapatite bone scaffolds with multi-scale porosity. Biomaterials 2007;28:45-54.

[31] Vitale-Brovarone C, Baino F, Tallia F, Gervasio C, Verné E. Bioactive glass-derived trabecular coating: a smart solution for enhancing osteointegration of prosthetic elements. J Mater Sci: Mater Med 2012;23:2369-80.

[32] Chen Q, Baino F, Pugno NM, Vitale-Brovarone C. Bonding strength of glass-ceramic trabecular-like coatings to ceramic substrates for prosthetic applications. Mater Sci Eng C 2013;33:1530-8

Figure legends

Fig. 1. SCNA scaffolds morphology and architecture: SEM micrographs at different magnification of (a) the surface (50×), (b) a transversal cross-section (120×) and (c) a strut with needle-shaped wollastonite crystals (2500×); (d) 3-D reconstruction of the scaffold volume (side 5 mm) by micro-CT and (e) mid-length cross-sections in the [xy], [xz] and [yz] orthogonal planes.

Fig. 2. Typical compressive stress-strain curve of SCNA scaffolds.

Fig. 3. Weibull plot for the compressive strength of SCNA scaffolds. The linear fitting parameters were defined in the Eq.(3) and were assessed through the least means squares algorithm. The plot is approximately linear over most of the stress range, but deviations from a linear relationship are apparent at low and high stress values, as commonly observed for such tests on other materials.

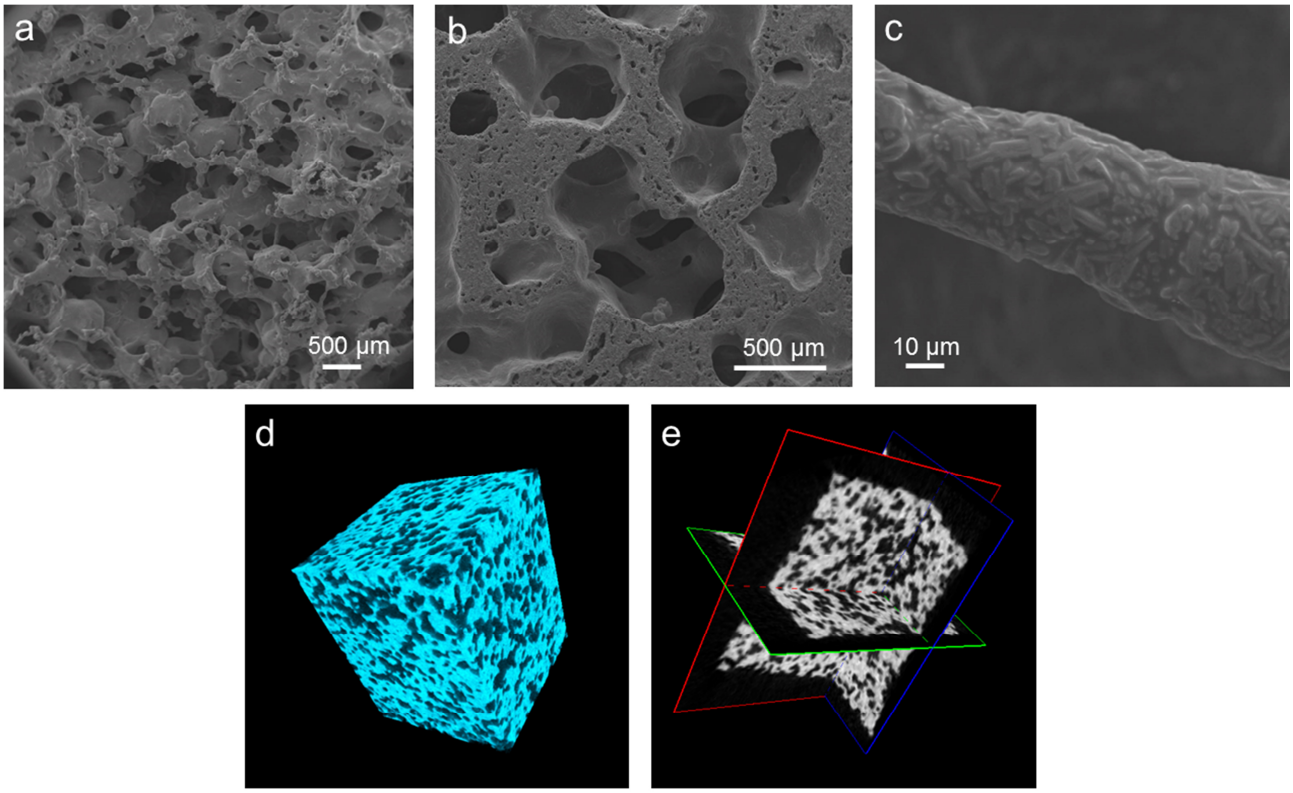

Fig. 1

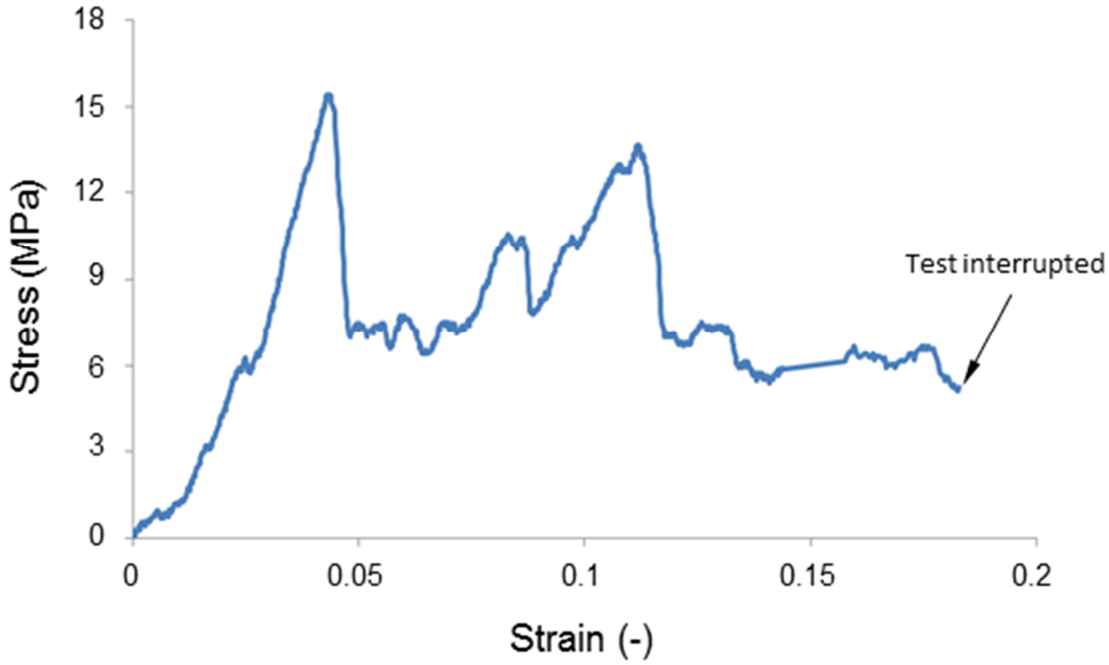
18
15
12
9
6
3
0
Stress (MPa)
0
0.05
0.1
0.15
0.2
Strain (-)
Test interrupted

Fig. 2

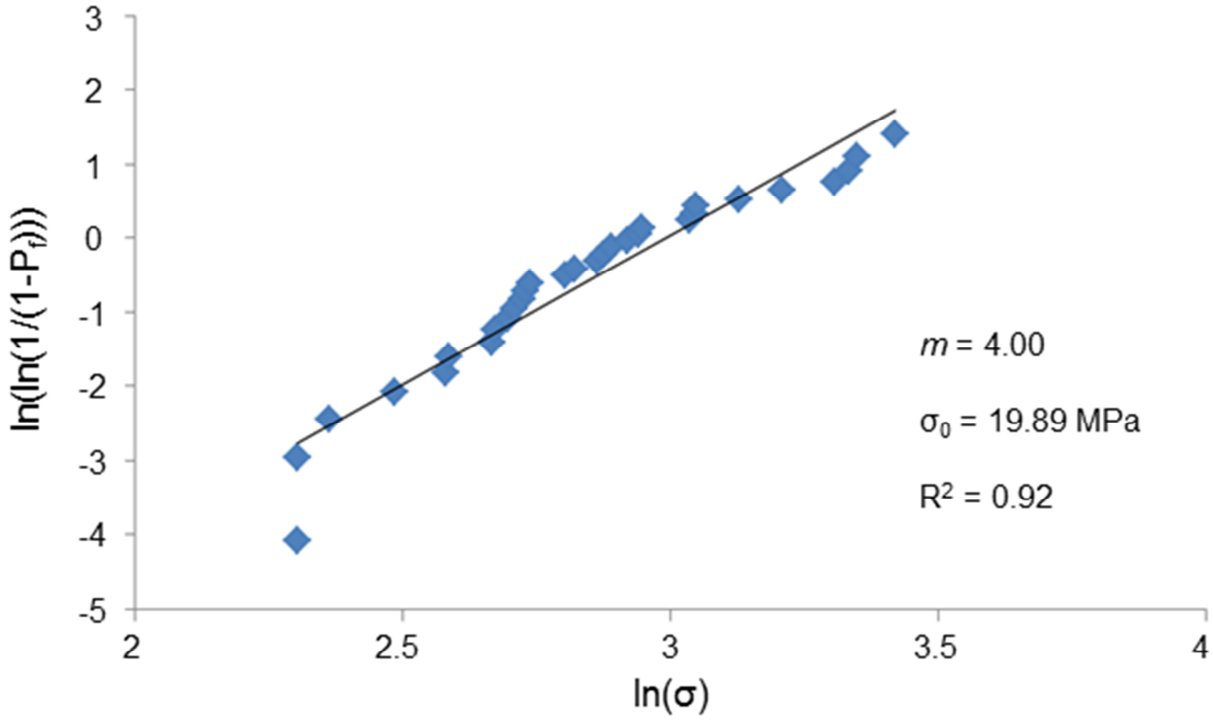

Fig. 3